

The Evolution of K^* and the Halo Occupation Distribution since $z = 1.5$: Observations vs. Simulations

Diego Capozzi ^{1*}, Chris A. Collins ¹, John P. Stott ^{1,2} and Matt Hilton ^{1,3}

1 - Astrophysics Research Institute, Liverpool John Moores University, Twelve Quays House, Egerton Wharf, Birkenhead, CH41 1LD

2 - Extragalactic & Cosmology Group, Department of Physics, University of Durham, South Road, Durham DH1 3LE

3 - School of Physics and Astronomy, University of Nottingham, NG7 2RD

Accepted ; Received ; in original form

ABSTRACT

We study the evolution of the K -band luminosity function (LF) and the halo occupation distribution (HOD) using Subaru observations of 15 X-ray clusters at $z = 0.8–1.5$ and compare the results with mock clusters ($0 < z < 1.3$) extracted from the Millennium Simulation and populated with galaxies by means of the semi-analytic model (SAM) of Bower et al., matched in mass to our observed sample. By fixing the faint-end slope ($\alpha = -0.9$), we find that the characteristic luminosity K^* defined by a Schechter LF is consistent with the predictions of the SAM, which are found, for the first time, to mimic well the evolution of K^* in rich clusters at $z \geq 1$. However, we cannot distinguish between this model and a simple stellar population synthesis model invoking passive evolution with a formation redshift ($z_f \simeq 5$) - consistent with the presence of an old red galaxy population ubiquitous in rich clusters at $z = 1.5$. We also see a small difference ($\Delta K^* \simeq 0.5$) between our clusters and studies of the field population at similar redshifts, which suggests only a weak dependence of the luminous ($L \geq L^*$) part of the LF on cluster environment. Turning to our study of the HOD, we find that within a radius corresponding to a density 500 times critical, high- z clusters tend to host smaller numbers of galaxies to a magnitude $K^* + 2$ compared to their low- z counterparts. This behavior is also seen in the mock samples and is relatively insensitive to the average mass of the cluster haloes. In particular, we find significant correlations of the observed number of member cluster galaxies (N) with both z and cluster mass: $N(M, z) = (53 \pm 1)(1+z)^{-0.61^{+0.18}_{-0.20}}(M/10^{14.3})^{0.86 \pm 0.05}$. Finally, we examine the spatial distribution of galaxies and provide a new estimate of the concentration parameter for clusters at high redshift ($c_g = 2.8^{+1.0}_{-0.8}$). Our result is consistent with predictions from both our SAM mock clusters and predictions of dark matter haloes from the literature. The mock sample predictions rise slowly with decreasing redshift reaching $c_g = 6.3^{+0.39}_{-0.36}$ at $z = 0$.

Key words: cosmology: large scale structure – galaxies: clusters: general – galaxies: evolution – galaxies: haloes – galaxies: luminosity function, mass function.

1 INTRODUCTION

The cold dark matter (CDM) paradigm is able to predict the formation of structures, which form through gravitational instabilities and cluster hierarchically. A way to study the structure formation, is by using the halo model formalism, according to which all galaxies in the Universe dwell in virialised units of mass called haloes

which obey universal scaling relations. N-body simulations (Navarro et al. 2004) show that dark matter haloes seem to have universal velocity and density profiles. The same cannot be said for galaxies, which are observed to be biased tracers of the mass distribution and whose clustering amplitude seems to depend on their properties. Studying the bias can provide insight into the physics of galaxy formation and the relationship between the galaxy and dark matter distributions, with the aim of uncovering the processes responsible for the way in which haloes, whose

* E-mail: dc@astro.livjm.ac.uk

properties are specified by the cosmological model, are populated with galaxies (Berlind & Weinberg 2002).

A fundamental tool for investigating the influence of bias on galaxy clustering statistics is the halo occupation distribution (HOD), generally used to determine the average number of galaxies within a dark matter halo as a function of the halo mass. Within the HOD framework, the virialised dark matter haloes with typical overdensities of $\Delta \sim 200$ (defined with respect to the critical density) are expected to be in approximate dynamical equilibrium and are described in one of three ways: (i) $P(N|M)$, the probability of a halo of given mass M having an average number of galaxies $\langle N \rangle$; (ii) the relation between galaxy and dark matter spatial distributions within haloes and (iii) the relation between galaxy and dark matter velocity distributions within haloes. Theoretical studies (e.g., Peacock & Smith 2000; Benson et al. 2000; Berlind & Weinberg 2002; Berlind et al. 2003; Kravtsov et al. 2004) based on N-body simulations, hydrodynamic simulations and semi-analytic models (SAMs) showed that $P(N|M)$ can be well modeled by a Poissonian distribution in the high halo mass regime ($M_h \gtrsim 10^{12} M_\odot$) while it assumes significant sub-Poissonian behavior, which can be modeled by a “nearest integer”¹ (N_{int}) distribution instead, for lower halo masses. These studies also showed $\langle N \rangle_M$ presents a sharp cutoff at low halo mass, a slowly rising plateau and a steep increase of the occupation number at high halo mass. A simple way to model the complicated shape of $\langle N \rangle_M$, avoiding the use of models involving a large number of parameters, is by assuming the existence of two separate galaxy populations within haloes: (i) central galaxies and (ii) satellite galaxies. This choice is motivated by reasons based on hydrodynamic simulations (Berlind et al. 2003) and on studies of observed galaxy clusters and groups, which take the brightest cluster galaxies (BCGs) as a different population from the rest of the cluster galaxies. These two populations can be modeled separately (e.g., Benson et al. 2000; Kravtsov et al. 2004; Zheng, Coil & Zehavi 2007), with the simplest case being modeling the HOD of central galaxies as a step function $\langle N_c \rangle = 1$ above a halo mass limit and a power law for satellite galaxies. In this way the HOD becomes a measure of the combined probability that a halo of mass M hosts a central galaxy and a given number N_s of satellite galaxies. Studies have also been carried out on the radial, spatial and velocity distributions of galaxies and dark matter, the majority of them focused on the latter. For instance, the halo concentration (defined as one of the shape parameters of the radial density profile) and its relation with mass and redshift have been the topic of many investigations in recent years (e.g. Nagai & Kravtsov 2005; Neto et al. 2007; Gao et al. 2008; Muñoz-Cuartas et al. 2011). The importance of the concentration resides in its connection with the mean density of the Universe at the time of collapse, i.e. more concentrated structures formed earlier in the past,

when the Universe was denser (Navarro, Frenk & White 1997 hereafter NFW, Neto et al. 2007; Gao et al. 2008; Muñoz-Cuartas et al. 2011). For this reason, understanding the dependence of concentration on mass and redshift and how the relationship between the concentration of dark matter and galaxies within haloes evolves with cosmic time, can provide fundamental insight into the formation and evolution of structures and into galaxy formation process.

Several statistical galaxy properties have been used to empirically measure the HOD assuming a power-law form ($\langle N \rangle_M \propto M^\beta$) for satellite galaxies. For instance, studies of the HOD have been carried out by using either the luminosity function (e.g., Yang, Mo & van den Bosch 2008), the spatial clustering (e.g., Phleps et al. 2006; Abbas et al. 2010) or by counting galaxies within known dark matter haloes, such as rich clusters (e.g., Kochanek et al. 2003; Lin, Mohr & Stanford 2004; Collister & Lahav 2005; Popesso et al. 2007; Ho et al. 2009). Our study focuses on this latter method, which is perhaps the most direct, using a sample of 15 X-ray selected clusters at high redshift.

Unfortunately, there is a significant disagreement among the results so far obtained and firm conclusions are hard to draw. For example, the slope of the $N - M$ relation is seen ranging between $\beta = 0.55$ (Marinoni & Hudson 2002) and $\beta \sim 1.7$ (Abbas et al. 2010); while the average concentration parameter of the galaxy density profile (c_g) is found to range between $c_g \sim 2$ and $c_g \sim 8$ (Carlberg et al. 1997; van der Marel et al. 2000; Biviano & Girardi 2003; Katgert, Biviano & Mazure 2004; Lin, Mohr & Stanford 2004; Rines & Diaferio 2006; Muzzin et al. 2007a; Biviano & Poggianti 2010). Although the majority of studies have been conducted at low redshift, these problems of consistency among different studies of the HOD extend to intermediate redshifts (e.g., Lin et al. 2006; Buote et al. 2007; Abbas et al. 2010), therefore there is a continuing motivation to investigate the evolution of the HOD with new galaxy samples.

The K -band LF can be used as a surrogate of the galaxy mass function because it is a sensitive probe of the bulk properties of galaxy populations out to $z \simeq 1.5$. There are several advantages to using the near-infrared light for such studies: i) K -band ($2.2 \mu\text{m}$) luminosities broadly reflect the total stellar mass of galaxies, resulting in a M/L ratio that is insensitive to the star-formation history of early-type galaxies; ii) stars are easy to remove, as they generally have $J - K < 1$ (Vega), whilst the k -correction makes the observed colours of the great majority of galaxies $J - K > 1$ (De Propris et al. 1999; McCracken et al. 2010); iii) k -correction in the near-infrared bands varies slowly with z and depends weakly on Hubble type (Poggianti 1997; Bruzual & Charlot 2003); iv) the effect of extinction at these wavelengths is significantly smaller than in optical and UV passbands. With the advent of infrared surveys like the *UKIRT Infrared Deep Sky Survey* (UKIDSS, Lawrence et al. 2007) and *Spitzer*, it has been possible to carry out studies of the stellar mass of high- z galaxies. However, such studies produced results in contrast with the prediction of SAMs. For instance, De Propris et al. (1999); Ellis & Jones (2004); Strazzullo et al. (2006) and Lin et al. (2006) studied

¹ Referred to as “Average” in Benson et al. (2000) and Berlind & Weinberg (2002). The definition of this distribution is $p(N_1|\langle N \rangle) = 1 - (\langle N \rangle - N_1)$, $p(N_1 + 1|\langle N \rangle) = \langle N \rangle - N_1$, where N_1 is the integer satisfying $N_1 \leq \langle N \rangle < N_1 + 1$, with $p(N|\langle N \rangle) = 0$ for all other values of N .

the evolution of the cut-off magnitude (K^*) of the cluster K -band LF out to $z \sim 1$ and found agreement with passive evolving models which have formation redshift ($z_f \sim 2 - 5$), suggesting that the bulk stellar mass of K^* cluster galaxies has not increased substantially since $z = 1$. Several other studies showed that the high-mass end of the galaxy mass function seems to remain pretty much unchanged since $z \sim 1$ for elliptical galaxies (e.g., Cimatti, Daddi & Renzini 2006 and Pozzetti et al. 2010) and similar results have been obtained for BCGs (Whiley et al. 2008; Collins et al. 2009 and Stott et al. 2010). These results suggest a timescale for the mass assemblage of galaxies similar to the age of their component stars, consistent with a monolithic-like model, and such activity can be viewed at least as qualitatively as consistent with a “downsizing” (Cowie et al. 1996; Thomas et al. 2005; De Lucia et al. 2007; Stott et al. 2007; Capozzi, Collins & Stott 2010 and references therein) process, according to which the more massive early-type galaxies end their star formation and settle on the colour-magnitude relation earlier than their less massive counterparts.

By contrast, the SAM used by De Lucia et al. (2006) predicts that the majority ($\simeq 70$ per cent) of the stellar mass of ellipticals at $z = 0$ is already formed by $z = 1$, but that at this redshift only a few per cent of this mass is assembled in the main progenitor.

In this paper we investigate the process of galaxy formation by studying the K -band LF (evolution of K^*) and the HOD of a sample of 15 galaxy clusters, containing the majority of the highest- z ($z > 0.8$) X-ray clusters observed so far. We want to push the study of the evolution of cluster galaxies to higher z by extending the Hubble diagram of K^* out to $z \sim 1.5$, because it is at $z \gtrsim 0.8$ that the differences among the evolutionary predictions based on stellar populations models are enhanced. The HOD of this sample is investigated using the number (N_{500}) of cluster galaxies within R_{500} (the radial distance where $\Delta = 500$) as a function of cluster mass and z . We also study galaxy clustering by analysing the radial galaxy surface number density profile in order to estimate the galaxy concentration parameter at $z \sim 1$ to compare with similar estimates at low z (e.g., Lin, Mohr & Stanford 2004). We compare the results of our HOD analysis with results obtained from dark matter haloes of similar redshift selected from the Millennium Simulation (MS; Springel et al. 2005), whose haloes are populated with galaxies taken from the SAM by Bower et al. (2006). It is worth pointing out that the majority of previous observation-based studies estimated c_g at low z (e.g., Lin, Mohr & Stanford 2004; Popesso et al. 2007), apart from some recent exceptions (Biviano & Poggianti 2010). In addition, even though more attention to the concentration parameter has been given by theoretical studies based on N-body simulations (e.g. Neto et al. 2007; Gao et al. 2008; Duffy et al. 2008) and SAM (Nagai & Kravtsov 2005), the majority of them focused more on c_{dm} (the concentration parameter of dark matter haloes’ radial density profiles) and its relation with halo mass and z . Here, instead, simulations and their associated SAMs are used to study the concentration of galaxies c_g . To our knowledge this is the first attempt to carry out a self-consistent comparison between the observed

galaxy concentration parameter in clusters and that in mock clusters within the MS.

The paper is organised as follows: in Section 2 we describe the observed cluster sample, while Section 3 is dedicated to data reduction and photometry. Sections 4 and 5 are focused on the study of the K -band LF and the HOD respectively of the observed and mock samples, while in Sections 6 and 7 we present and discuss our results. Finally, we draw our conclusions in Section 8.

Throughout this paper we make use of magnitudes in the Vega photometric system and assume a standard cosmology with $H_0 = 70 \text{ km s}^{-1} \text{ Mpc}^{-1}$, $\Omega_m = 0.3$ and $\Omega_\Lambda = 0.7$.

2 CLUSTER SAMPLE

The clusters are a subsample of the cluster sample described in Stott et al. (2010) and consist of the clusters from that list with available J and K band data. Two clusters (CL J1226+3332, Maughan et al. 2004, and MS1054.4-0321, Branchesi et al. 2007) were included in the original sample, but we decided to exclude them because the *MOIRCS* field of view (FOV) ($4' \times 7'$) (see below) was not extended enough to contain their large R_{500} . Our final sample consists of the 15 clusters between $0.8 < z < 1.5$ detailed in Table 1. Some of these were discovered by various X-ray surveys whilst some were optically selected clusters showing extended X-ray emission. All 15 clusters have spectroscopically confirmed redshifts (Fig. 1) and X-ray luminosities in the range $1 < L_X < 19 \times 10^{44} \text{ erg s}^{-1}$. Cluster mass estimates are made using the $M - T_X$ relation in Stott et al. (2010), whose parameter values are based on the Maughan (2007) derived $M - T_X$ relation. We refer to the study by Stott et al. (2010) for further details about the derivation of cluster masses.

3 OBSERVATIONS, DATA REDUCTION AND PHOTOMETRY

The observations were taken with the *MOIRCS* camera (Ichikawa et al. 2006) on the 8.2 m *Subaru* telescope, which provides imaging and low-resolution spectroscopy over a total FOV of $4' \times 7'$ with a pixels scale of $0.117''$ per pixel. Observations were taken in $0.5''$ seeing on the nights of August 8th and 9th 2007 and in $0.3'' - 0.6''$ seeing on the nights of December 16th 2008 and April 18th 2009, with the clusters centered on Detector 2. A circular 11-point dither pattern of radius $25''$ was used for both bands to ensure good sky-subtraction. The modal integration times were 25 min at J and 21 min at K_s , although we observed some of the higher redshift clusters for 50 per cent longer when scheduling allowed. These exposures reach a 5σ limiting magnitude of at least $J=21$ and $K_s = 20$ (Vega).

The data are reduced using the external IRAF package MCSRED. They are flat-fielded, sky subtracted, corrected for distortion caused by the camera optical design and registered to a common pixel coordinate system. The final reduced images on which we perform the photometry are made by taking the 3σ (s.d.) clipped mean of the

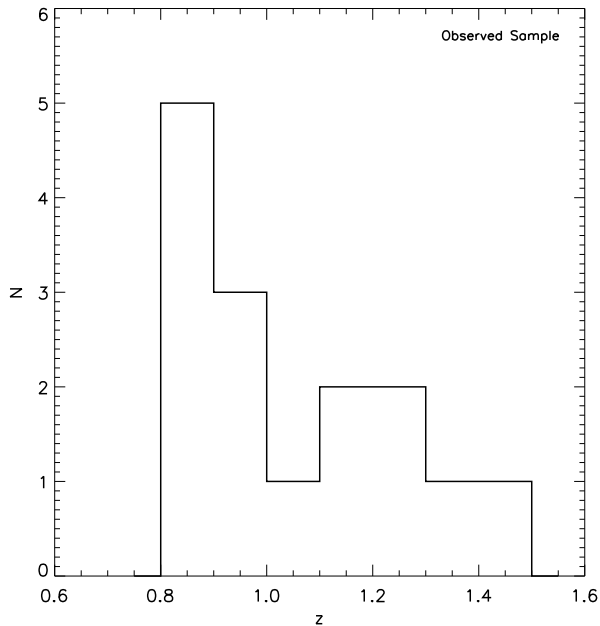


Figure 1. Spectroscopic redshift distribution of the 15 observed clusters in our sample.

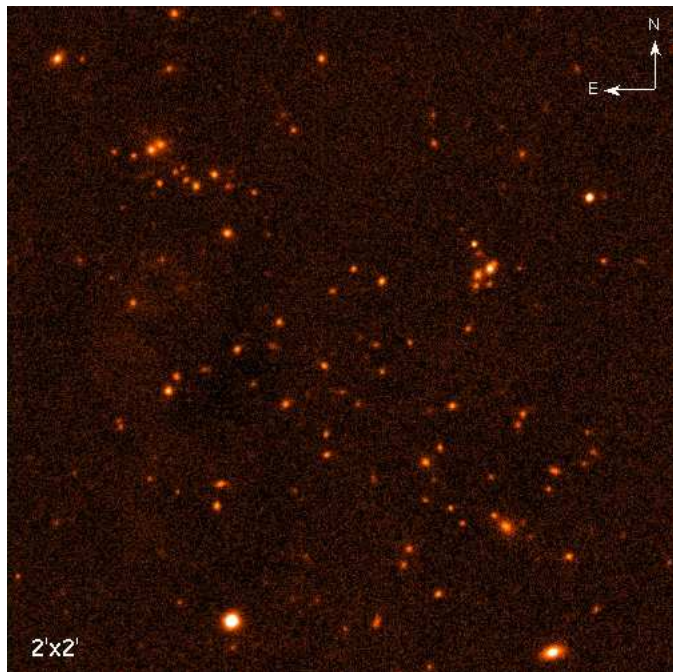


Figure 2. $2' \times 2'$ K -band image of CL J0152.7-1357

dither frames. The galaxy photometry is extracted using SExtractor (version 2.5) MAG_AUTO magnitude, which is found to be within ~ 0.1 mag of the total for extended sources (Martini 2001). To calculate the colours of the galaxies, we run SExtractor in dual image mode so that the K_s (hereafter K , for simplicity) band detections extract the J band catalogue with identical positions and apertures

to ensure accurate colour determination. This photometry is carried out by using SExtractor MAG_APER magnitude using a circular aperture of diameter $1''$.

The photometry is calibrated to the Vega system using a combination of standard star observations and the *Two Micron All Sky Survey* (2MASS, Skrutskie et al. 2006) and UKIDSS catalogues. The typical photometric errors are 0.01 and 0.08 for the standard star and survey calibrated data, respectively.

In Figure 2 the image of CL J0152.7-1357 obtained after all the described process is shown as an example.

4 ANALYSIS OF THE OBSERVED CLUSTER SAMPLE

In order to carry out our study of the LF and the HOD, both foreground and background objects have to be removed or accounted for. It is well known (e.g., Leggett 1992; De Propris et al. 1999) that stars generally have observed $J - K < 1$ (Vega), while, because of k -correction, the great majority of galaxies, excluding the most local ones, lie in the region $J - K > 1$. Carrying out such a colour cut effectively removes contamination by stars. However, there is the possibility that faint blue galaxies have observed $J - K < 1$, so for this reason we only perform this $J - K < 1$ at magnitudes brighter than $K = 18$, i.e. at least 2 mag brighter than the 5σ limit of each cluster. Fainter than this, field galaxy counts outnumber those of the stars by more than a factor of 10 (De Propris et al. 1999; McCracken et al. 2010), thus at these faint magnitudes the correction for stellar contamination becomes relatively unimportant. From simulations we estimate a contamination of only 3–4 stars per cluster at $K < 18$, which remains stable down to a 4σ detection limit.

The correction for foreground and background galaxies is performed statistically using the *UKIDSS Ultra Deep Survey*² (UDS) Data Release 5 field. This field consists of a region of $A = 0.77$ sq. deg in the northern hemisphere with a 5σ depth of 21.5 and 22.5 in K and J bands, respectively. For reasons of homogeneity, the same method is used for carrying out the star-galaxy separation in the background field.

For all galaxies in this field, sky coordinates, total magnitudes and aperture magnitudes (used to calculate galaxy colours) are extracted from the UDS database.

4.1 K -Band LF

The cluster sample is divided into three redshift bins (median $z=0.85, 0.97, 1.23$) roughly containing the same number of clusters. For each cluster, after the stars are removed, we determine the K -magnitude distribution binned in 0.5-mag intervals. The number of galaxies in each bin N_{bin} is calculated using the formula (Ellis & Jones 2004):

$$N_{bin} = N_{cl} - N_{back} \left(\frac{A_{cl}}{A_{back}} \right), \quad (1)$$

² A detailed description of the survey can be found at: <http://www.nottingham.ac.uk/astronomy/UDS/>.

Name	RA	Dec	z	T_x (keV)	M_{200} ($10^{14} M_\odot$)	Reference
RDCS J1317 + 2911	13:17:21.70	+29:11:18.0	0.81	$4.0^{+1.3}_{-0.8}$	$2.7^{+2.9}_{-1.3}$	Branchesi et al. (2007)
CL J0152.7 - 1357	01:52:41.00	-13:57:45.0	0.83	$5.4^{+0.9}_{-0.9}$	$4.5^{+2.7}_{-2.2}$	Vikhlinin et al. (2009)
CL J1559.1 + 6353	15:59:06.00	+63:53:00.0	0.85	$4.1^{+1.4}_{-1.0}$	$2.8^{+3.2}_{-1.5}$	Maughan et al. (2006)
CL J1008.7 + 5342	10:08:42.00	+53:42:00.0	0.87	$3.6^{+0.8}_{-0.6}$	$2.2^{+1.6}_{-1.0}$	Maughan et al. (2006)
CL 1604 + 4304	16:04:25.20	+43:04:53.0	0.9	$2.5^{+1.1}_{-1.0}$	$1.2^{+1.6}_{-0.6}$	Lubin, Mulchaey & Postman (2004)
CL J1429.0 + 4241	14:29:06.40	+42:41:10.0	0.92	$6.2^{+1.5}_{-1.0}$	$5.5^{+3.3}_{-2.0}$	Maughan et al. (2006)
RCS J0439 - 2904	04:39:38.00	-29:04:55.0	0.95	$1.5^{+0.3}_{-0.2}$	$0.5^{+0.4}_{-0.2}$	Hicks et al. (2008)
2XMM J083026 + 524133	08:30:25.90	+52:41:33.0	0.99	$8.2^{+0.9}_{-0.9}$	$8.5^{+4.1}_{-3.4}$	Lamer et al. (2008)
WARPS J1415.1 + 3612	14:15:11.10	+36:12:03.0	1.03	$6.2^{+0.8}_{-0.7}$	$5.2^{+2.9}_{-1.9}$	Branchesi et al. (2007)
RDCS J0910 + 5422	09:10:44.90	+54:22:09.0	1.11	$6.4^{+1.5}_{-1.2}$	$5.3^{+4.1}_{-2.5}$	Balestra et al. (2007)
RX J1053.7 + 5735 (West)	10:53:39.80	+57:35:18.0	1.14	$4.4^{+0.3}_{-0.3}$	$2.7^{+1.4}_{-1.0}$	Hashimoto et al. (2004)
XLSS J022303.0 - 043622	02:23:03.00	-04:36:22.0	1.22	$3.5^{+0.4}_{-0.4}$	$1.8^{+0.9}_{-0.7}$	Stott et al. (2010), Bremer et al. (2006)
RDCS J1252.9 - 2927	12:52:54.40	-29:27:17.0	1.24	$7.2^{+0.4}_{-0.6}$	$6.1^{+2.3}_{-2.4}$	Balestra et al. (2007)
XMMU J2235.3 - 2557	22:35:20.60	-25:57:42.0	1.39	$8.6^{+1.3}_{-1.2}$	$7.7^{+4.4}_{-3.1}$	Rosati et al. (2009)
XMMXCS J2215.9 - 1738	22:15:58.50	-17:38:03.0	1.46	$4.1^{+0.6}_{-0.9}$	$2.1^{+1.9}_{-0.8}$	Hilton et al. (2010)

Table 1. The observed cluster sample.

where N_{cl} and A_{cl} represent the number of cluster galaxies and the cluster area respectively; while N_{back} and A_{back} are the corresponding numbers for the background field.

The corresponding error in each bin interval is found by summing in quadrature the Poissonian error on N_{cl} and the error on the background - which is made up of a Poissonian term and a term accounting for galaxy clustering and given by

$$\sigma_{N_{back}} = \sqrt{N_{back}} \sqrt{1 + \frac{2\pi N A_{cl} \theta_c^{2-\delta}}{2-\delta}}. \quad (2)$$

Here θ_c is the angular radius such that $\Omega = \pi\theta_c^2$, Ω being the solid angle of the background field, and N is the number density of galaxies in the bin considered. The error on N_{back} is then normalised to the projected surface area of the cluster. The parameters δ and A_{cl} describe the galaxy angular correlation function such that:

$$\omega(\theta) = A_{cl}\theta^\delta. \quad (3)$$

We adopt the values $\delta = -0.8$ and $A_{cl} = (13.49 \pm 1.57) \times 10^{-4}$ taken from Temporin et al. (2008), who studied the K -band angular correlation function down to $K = 20.5$, using the *VIMOS VLT Deep Survey*³ (VVDS).

Similarly to De Propris et al. (1999), we then use the difference in redshift between the cluster redshift and the median redshift of its assigned bin, along with the k -correction, to appropriately transform the galaxy magnitudes. In this way, the intervals will align at the median redshift of each bin. The k -correction is calculated by using the model of Bruzual & Charlot (2003).

For each redshift bin, we obtain a stacked luminosity function (Fig. 3). BCGs are excluded, as they affect the LFs in such a way that the abundance of very bright galaxies is underestimated when a Schechter function is used for the fitting (e.g., Schechter 1976; Christlein & Zabludoff 2003). We then fit the stacked LFs obtained in each bin with a

Schechter function (Schechter 1976), fixing the faint end slope to $\alpha = -0.9$, under the supposition this parameter does not evolve with cosmic time and solving for both K^* and the normalization. This is the value of α measured by De Propris et al. (1998) for the K -band LF of the Coma Cluster at $z \sim 0.02$. The choice of fixing α is justified by our photometry only reaching ~ 1.5 mag below L^* . The fitting procedure was based on least-squares based on the the Levenburg-Marquardt algorithm. The values of the best fit K^* for the stacked LFs are reported in Table 2, while the best fit LFs (plotted as average galaxy number counts per cluster vs. magnitude) are shown in Figure 3.

Since the value of α measured in the field is $\alpha \sim -1$ (Cirasuolo et al. 2010) we also repeat the fit for the stacked LF fixing the slope to $\alpha = -1$. The best fit values of K^* obtained (Table 2) are consistent within 1σ of the ones corresponding to $\alpha = -0.9$. The latter values are plotted in the Hubble diagram in Figure 4, together with the predictions of evolutionary models with different formation z calculated using the Bruzual & Charlot (2003) model. The models are calculated assuming a simple stellar population (SSP) with a Chabrier initial mass function and solar metallicity. In Figure 4 we also compare our results with the predictions of the SAM by Bower et al. (2006), which implements baryon physics, such as AGN feedback from a central black hole and star formation, as a SAM bolted onto the MS. Mock clusters were selected from the simulations in seven redshift snapshots as described in Section 5. The K^* values from the mock clusters are obtained by applying identical selection criteria to the real data, including the same least-squares fitting procedure.

4.2 HOD Analysis

Despite the diverse methods for studying the HOD, directly counting the number of galaxies within known dark matter haloes remains the most straightforward way to estimate the average galaxy number within a halo as a function of halo mass. Furthermore, for galaxy clusters their total mass can be estimated via gravitational lensing or, as in this case, us-

³ Detailed information about this survey can be found at: <http://www.oamp.fr/virmos/vvds.htm>.

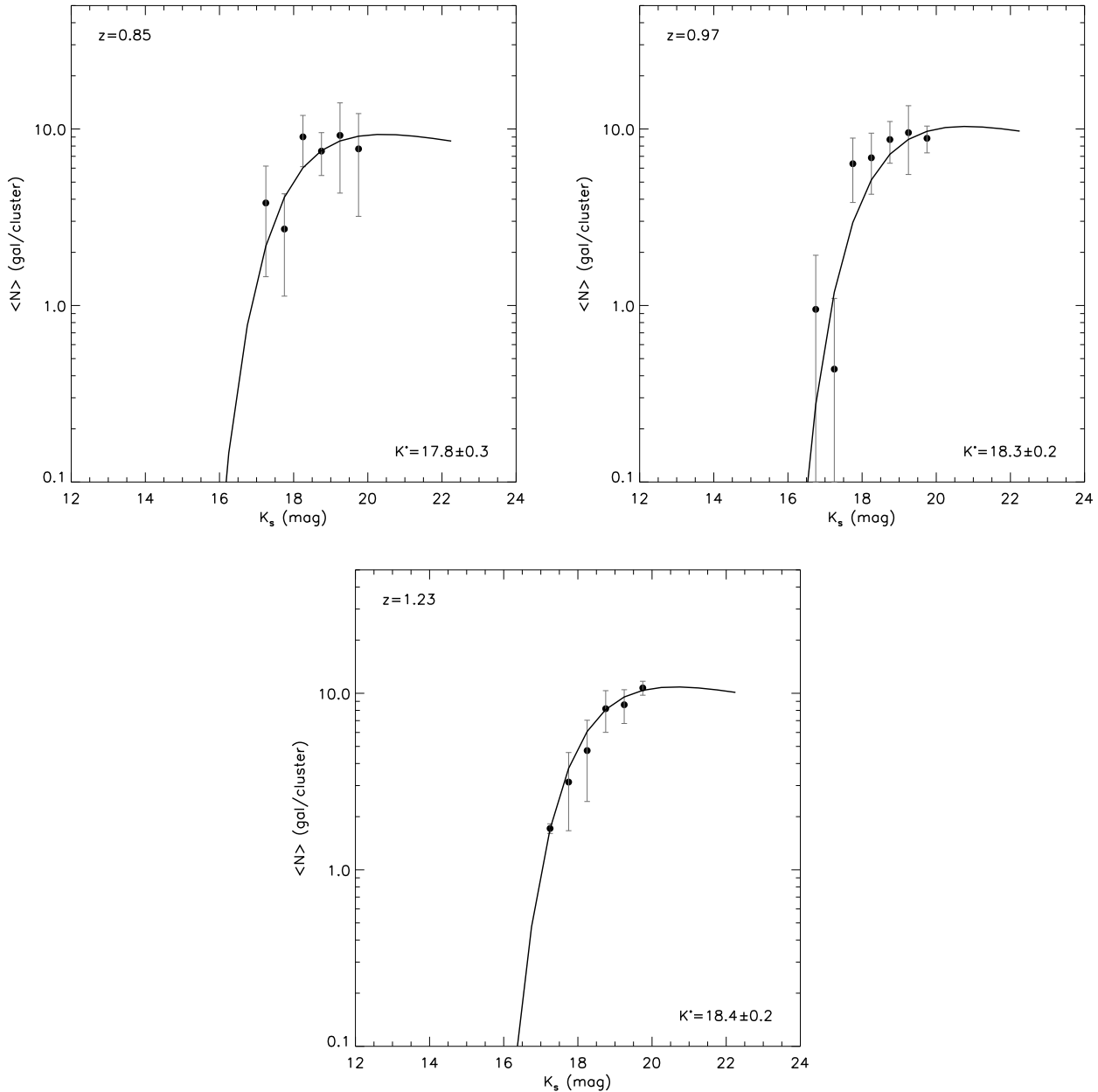


Figure 3. K -band stacked LFs for our three z bins ($z = 0.85, 0.97, 1.23$) with their best-fitting values of K^* .

ing the temperature of the X-ray emitting gas sitting in the cluster's gravitational potential well. Estimating the halo masses in such a way can constrain quite directly $P(N|M)$ at high mass (Berlind & Weinberg 2002). Furthermore, the relation between dark matter and galaxy spatial distributions can be investigated in clusters by means of the radial distribution of their galaxies. The latter can be directly probed by their surface density profile.

As mentioned before in Section 1, several studies (e.g. Berlind & Weinberg 2002; Kravtsov et al. 2004) have shown that $\langle N \rangle_M$ can be described as the joint probability that a halo of mass M hosts a central galaxy and that the halo hosts a given number N_s of satellite galaxies. Since this study in-

vestigates the high mass regime of $\langle N \rangle_M$, where $P(N|\langle N \rangle)$ is expected to be Poisson distributed, only satellite cluster galaxies are considered; moreover the observed and mock clusters analysed here always have $M_{200} > 10^{14} M_\odot$ where, as described in the Introduction, $\langle N \rangle_M \propto M^\beta$. In addition these clusters (mock and real) are also used to study c_g at high redshift. We note here that in order to directly compare our results with those of other workers we transform from M_{200} and R_{200} to the respective values at over density 500. In this paper the mass transformation is always carried out using the standard NFW profile prescription by Hu & Kravtsov (2003) and for the radial scaling we use

z	K^* ($\alpha = -0.9$)	K^* ($\alpha = -1$)	$\langle M_{500} \rangle$ ($10^{14} M_{\odot}$)	$\langle N_{500} \rangle$ (gal)	No. Clusters
0.85	17.8 ± 0.3	17.4 ± 0.6	2.0 ± 0.4	48 ± 8	5
0.97	18.3 ± 0.2	18.0 ± 0.6	3.6 ± 1.2	56 ± 7	4
1.23	18.4 ± 0.2	18.6 ± 0.3	3.1 ± 0.7	46 ± 6	6

Table 2. Here are tabulated, for each redshift bin, the values of median z (col 1), best-fitting K^* for $\alpha = -0.9$ (col 2), best-fitting K^* for $\alpha = -1$ (col 3), average galaxy number within R_{500} (col 4) and number of clusters per z bin (col 5), measured for our observed cluster sample.

$M_{\Delta} = (4/3)\pi R_{\Delta}^3 \Delta \rho_c(z)$, where Δ is the considered overdensity.

4.2.1 $N_{500} - M_{500}$ Relation

After determining the values of K^* for each of the three redshift bins, we are able to calculate $\langle N_{500} \rangle$ to a depth of $K = K^* + 1.5$. However, in order to allow us to meaningfully compare our results with other studies at low z , where at least a depth of $K = K^* + 2$ is reached, we decided to extrapolate $\langle N_{500} \rangle$ to $K^* + 2$ (after normalising brighter than $K = K^* + 1.5$ and allowing for suitable propagation of errors). The values obtained are shown in Table 2. We plot these values against M_{500} together with Lin, Mohr & Stanford (2004) data points and best-fit relation at $z \sim 0.06$ in Fig. 5.

4.2.2 Galaxy Surface Density Profile

After selecting only cluster galaxies (BCGs excluded) within $R/R_{500} < 1$ and out to $K = K^* + 1.5$, we stack them all to obtain a single radial profile. We then calculate the surface number density normalised per virial area and plot it as a function of virial fraction (R/R_{200}). In this way we are able to obtain a stacked radial number density profile and to study the mean concentration of cluster galaxies at $z \sim 1$. In order to estimate c_g we fit a NFW density profile to the data. The three-dimensional NFW profile has the following form:

$$\frac{\rho(r)}{\rho_c} = \frac{\delta_c}{(r/r_s)(1+r/r_s)^2}, \quad (4)$$

where $\rho_c = 3H_0^2/8\pi G$ is the critical density for closure, δ_c is a characteristic density contrast and r_s is a scale radius. Since we consider a density contrast of $\Delta = 200$, δ_c and r_s take the following form,

$$\delta_c = \frac{(200/3)c^3}{[\ln(1+c) - c/(1+c)]}, \quad (5)$$

$$r_s = r_{200}/c, \quad (6)$$

where c is the concentration parameter of the profile. The surface density is then obtained by projecting the three-dimensional profile along the line of sight from negative to positive infinity and, following Bartelmann (1996), can be written as

$$\Sigma(x) = \frac{2\rho_s r_s}{x^2 - 1} f(x), \quad (7)$$

where $\rho_s = \delta_c \rho_c$, $x = cr/r_{200}$ and $f(x)$ is given by:

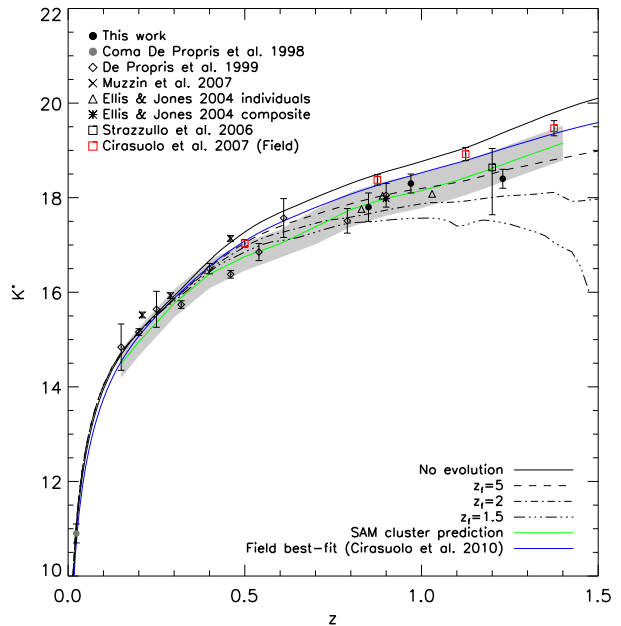


Figure 4. Hubble diagram for K^* . The data points for the cluster environment are taken from: this work, De Propriis et al. (1998, 1999), Muzzin et al. (2007a), Ellis & Jones (2004) and Strazzullo et al. (2006). From the field: Cirasuolo et al. (2007). Several evolutionary models are also plotted: no evolution in absolute K -band magnitude (full line), passive evolution with $z_f = 1.5, 2$ and 5 (dashed-triple-dotted, dashed-dotted and dashed line respectively) and Bower et al. (2006) SAM predictions (green full line) obtained by using mock clusters (see text). The grey-shaded region shows the typical variation in the evolution of the SAM K^* when a constant halo cluster mass is adopted. The scatter is dominated by Poisson statistics. The parametrization of the observed evolution of the field K^* by Cirasuolo et al. (2010) is also shown (blue full line).

$$f(x) = \begin{cases} 1 - \frac{2}{\sqrt{x^2-1}} \arctan \frac{\sqrt{x-1}}{\sqrt{x+1}} & (x > 1), \\ 1 - \frac{2}{\sqrt{1-x^2}} \operatorname{arctanh} \frac{\sqrt{1-x}}{\sqrt{1+x}} & (x < 1), \\ 0 & (x = 1). \end{cases} \quad (8)$$

The limited FOV of *MOIRCS* does not allow us to observe galaxies far enough from the cluster to be able to determine the background level by investigating regions of the sky dominated by field galaxies. For this reason, and because we do not have spectroscopic redshifts for our cluster galaxies, we can not directly background subtract our stacked number density profile. Hence we start with the methodology of Lin, Mohr & Stanford (2004) and carry out a maximum likelihood fit to the projected radial density profile with the supposition of having a constant background. The observed profile is binned very finely in virial fraction (R/R_{200}) so that in every bin, the density within the differential area dS could be considered constant. By doing this we can estimate the probability of obtaining the measured galaxy counts within dS for a specific prediction (N_{model}) given by the model. This situation is well represented by a Poisson probability distribution with mean $\lambda = N_{\text{model}}$. Our model is simply given by the sum of the cluster contri-

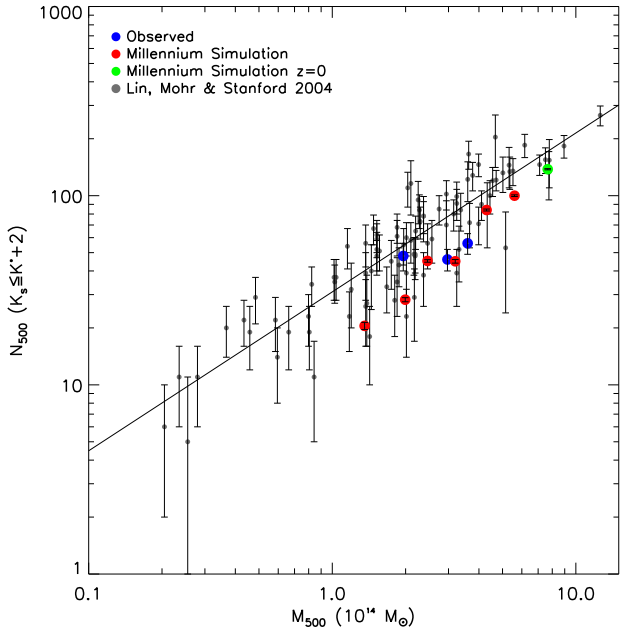


Figure 5. N_{500} against M_{500} . Our mean values are reported as blue full dots (observed sample), red full dots (mock clusters with $z > 0$) and green full dot (mock clusters at $z = 0$). Note that the observed data point at $z = 1.23$ has been slightly shifted towards lower masses to make it visible. The data points of Lin, Mohr & Stanford (2004) –plotted as grey full dots– together with their best-fitting relation are shown. We note that, since Lin, Mohr & Stanford (2004) values are measured over clusters at $z \sim 0.06$, only the average value for N_{500} at $z = 0$ (green full dot) can be directly compared with them. Note our simulation-based measures are average values measured over the 100 most massive clusters in each snapshot (see text).

tribution to the projected density and the contribution of the background:

$$\Sigma = \Sigma_{cl} + \Sigma_{back}, \quad (9)$$

where Σ_{cl} is given by eq. 7 and Σ_{back} is a constant. Specifically, the quantity

$$-\log \mathcal{L} = - \sum_1^{N_{bin}} \log \left[\frac{e^{-\lambda_i} \lambda_i^{N_{obs_i}}}{N_{obs_i}!} \right], \quad (10)$$

is minimised, where N_{bin} is the number of bins used, N_{obs_i} is the observed number counts in the differential area dS_i and $\lambda_i = \Sigma(x_i)dS_i$ is the number of galaxies predicted by the model (cluster galaxies plus background, N_{model}) in the same differential area as a function of ρ_s , $c = c_g$ and Σ_{back} . In the fitting routine we allow the parameters ρ_s , c_g and Σ_{back} to vary. The advantage of this method is that the likelihood involves a proper sum of Poisson probabilities (in this respect our method improves on the one used by Lin, Mohr & Stanford 2004) and that, unlike methods based on the χ^2 , the results are relatively independent of the binning. Figure 6 shows the stacked radial density profile out to $\sim 0.65R_{200}$ corresponding to the R_{500} radius considered for each cluster. The determined best fitting galaxy concentration parameter is $c_g = 2.8_{-0.8}^{+1}$, with the uncertainties derived from the relation $\Delta\chi^2 = -2\Delta \log \mathcal{L}$. The value

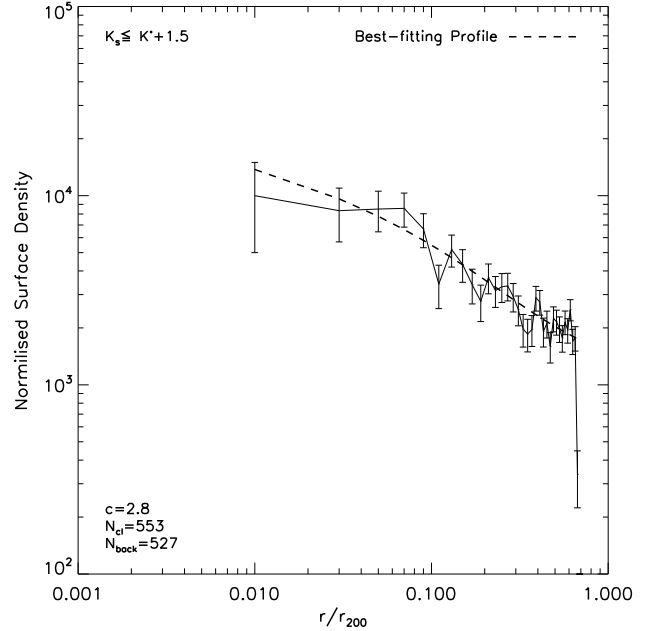


Figure 6. Stacked radial surface number density profile for our observed cluster sample. Galaxies within R_{500} and out to $K = K^* + 1.5$ only are used. The best-fitting profile is shown as a dashed line.

obtained is consistent with those found by Carlberg et al. (1997), van der Marel et al. (2000), Lin, Mohr & Stanford (2004) and Biviano & Poggianti (2010) for clusters at low and intermediate redshifts ($c_g = 3.7, 4.2, 2.9$ and 4.0 at $z \sim 0.3, 0.3, 0.1$ and 0.55 , respectively). We must point out though, that the magnitude limit used in these studies does not always coincide with ours.

The background density obtained amounts to around $\Sigma_{back} \sim 8$ per cent of the peak density of the stacked profile or $\simeq 49$ per cent of total galaxies (527 out of 1080). We tested the reliability of these estimates by analysing the radial number density profile out beyond R_{200} . This is done by using those clusters in the sample (3 out of 15) whose R_{200} is small enough to allow us to estimate the background out to at least $1.4R_{200}$. For these clusters the background level is evaluated by averaging the values in the outermost bins ($R/R_{200} > 1$) of the radial profile. The values obtained vary between 4 and 12 per cent of the density peak value, corresponding to 30–50 per cent of the total galaxy number out to the same radial distance as used in the stacked profile ($R \simeq 0.65R_{200}$). This result is in relatively good agreement with the background level estimated with the likelihood.

5 ANALYSIS OF MOCK CLUSTER SAMPLES

5.1 Cluster Halo Selection

The MS⁴ is a large N-body simulation of the standard Λ CDM cosmogony. It follows 2160³ particles, each of mass

⁴ Detailed information about the simulation can be found at: <http://www.mpa-garching.mpg.de/millennium/>. A de-

Redshift	β	$\langle M_{500} \rangle$ ($10^{14} M_{\odot}$)	$\langle N_{500} \rangle$ (gal)	c_g	c_{dm}	$\Delta \log c$
0	0.82 ± 0.01 (3769)	7.6 ± 0.3	138 ± 1	$6.30^{+0.39}_{-0.36}$	3.74	$0.23^{+0.03}_{-0.02}$
0.21	0.76 ± 0.01 (2752)	5.6 ± 0.2	100 ± 1	$5.31^{+0.39}_{-0.35}$	-	-
0.41	0.82 ± 0.02 (1953)	4.3 ± 0.1	84 ± 1	$5.05^{+0.41}_{-0.38}$	-	-
0.62	0.86 ± 0.02 (1289)	3.2 ± 0.1	45 ± 1	$4.90^{+0.52}_{-0.47}$	3.48	$0.15^{+0.05}_{-0.04}$
0.83	0.74 ± 0.03 (831)	2.4 ± 0.1	45 ± 1	$3.85^{+0.45}_{-0.40}$	-	-
0.99	0.78 ± 0.04 (541)	2.0 ± 0.1	28 ± 1	$3.70^{+0.50}_{-0.44}$	3.66	$0.00^{+0.06}_{-0.05}$
1.27	0.81 ± 0.08 (233)	1.40 ± 0.05	21 ± 1	$3.77^{+0.58}_{-0.51}$	-	-

Table 3. Properties of the mock cluster sample. Col1: redshift of the snapshot bin; col2: the slope β of the $N_{500} - M_{500}$ relation (HOD power-law index) for all the mock clusters in the snapshot with the number of clusters shown in parenthesis - note that all other estimates from the mock sample in this table use the 100 most massive cluster haloes at each redshift snapshot; col3: the average mass within the radius corresponding to $\Delta = 500$; col4: the average galaxy number within R_{500} brighter than $K^* + 2$ (these values do not include the systematic correction of 10 per cent discussed in Section 5.2); col5: the average galaxy concentration parameter for the mock clusters; col6: the average dark matter concentration parameter as measured from the $c_{dm}(M, z)$ relation of Gao et al. (2008), not available for all z ; col9: $\Delta \log c = \log(c_g/c_{dm})$, see text.

$8.6 \times 10^8 h^{-1} M_{\odot}$, in a cubic box of $500 h^{-1}$ Mpc on a side from redshift $z = 127$ to the present. The cosmological parameters were chosen to be consistent with a combined analysis of the 2dFGRS (Colless et al. 2001; Percival et al. 2001) and first-year *Wilkinson Microwave Anisotropy Probe* (*WMAP*) data (Spergel et al. 2003) within the concordance cosmology.

By scanning the entire volume of the simulations we extract all haloes above a minimum mass of $M_{200} > 10^{14} M_{\odot}$, selected in seven snapshots corresponding to redshifts $z = 0, 0.21, 0.41, 0.62, 0.83, 0.99$ and 1.27 , respectively.

The purpose of the simulations is to follow the evolution of the observed clusters, which do not constitute a statistical sample but are highly biased to the most X-ray luminous systems and therefore the most massive clusters at $z > 0.8$. The finite volume of the MS means that the number of massive clusters is rare, so for the study of the evolution of K^* , $\langle N_{500} \rangle$ and c_g , we restrict our analyses to the most massive cluster haloes in each snapshot of the simulation, since they are thought of as equivalent to the brightest X-ray systems. This approach follows that of De Lucia & Blaizot (2007) who used the 125 most massive clusters in similar snapshot intervals from the MS to investigate the evolution of BCGs in X-ray selected luminous clusters (see Sect. 6 of their paper). Selecting the most massive 100 clusters per snapshot we can reproduce both the observed redshift and mass distributions of our high-redshift clusters reasonably well; for the mocks: $0.83 < z < 1.27$, $1 < M_{500} < 7.7 \times 10^{14} M_{\odot}$ and median $M_{500} = 1.8 \times 10^{14} M_{\odot}$, and for the observations: $0.81 < z < 1.46$, $0.4 < M_{500} < 6.2 \times 10^{14} M_{\odot}$ (next least massive cluster is at $0.9 \times 10^{14} M_{\odot}$, so only one observed cluster lies significantly outside the mock mass range), and median $M_{500} = 2 \times 10^{14} M_{\odot}$. Details of the mock clusters used are given in Table 3.

One consequence of selecting the most massive haloes per snapshot is that the mass range evolves with cosmic time (as in the analysis of De Lucia & Blaizot 2007), so to investigate whether our results are biased by this mass

evolution we also present results using other mock cluster samples selected with a constant average mass and a constant mass range over cosmic time. Results of these analyses are reported in Section 6.2.3. The galaxies populating the haloes used are extracted from the SAM (see also Section 4.1) galaxy catalogue by Bower et al. (2006).

5.2 Satellite Galaxies' Power-law Index & Occupation Number

Once the galaxy spatial coordinates and K -band magnitude are extracted for the totality of haloes contained in each redshift bin, we select galaxies with projected radial distances within R_{500} for each mock catalogue and carry out individual fits to obtain individual LFs in the same way as described for the observations in Section 4.1. We point out that in order to reproduce observations the cut in R_{500} is not applied along the line of sight and that galaxies are assigned to each halo by using the unique halo IDs, which allow us to univocally associate galaxies to the haloes they belong to. However, on larger scales the lack of a background in the mocks means that the galaxy selection differs from the observed clusters, for which galaxies are counted within a cylinder of projected radius R_{500} and a background correction applied using galaxy counts (see Section 4.1). In principle line-of-sight contamination from galaxy clustering on scales extending beyond the virial radius of the clusters could affect our richness and concentration values by introducing an offset between measured and mock estimates. Therefore to check this we inspect the number of non-cluster galaxies at $z = 1$ brighter than $K^* + 2$, with physical and projected distances from mock halo central galaxies of $R_{500} < R < 3$ Mpc and $R < R_{500}$ respectively. We find that N_{500} values for the mock clusters are $\simeq 10$ per cent lower on average compared to those observed due to this contamination. This is less than the individual Poisson error on N_{500} for each cluster. From an observational perspective these results are broadly consistent with De Filippis et al. (2011) who compared what effect local and global background corrections have on the counts in clusters at low redshift.

The radial distances for the mock sample are calculated

tailed description of the data base can be found in Lemson & Virgo Consortium (2006).

with respect to the central galaxy of the halo, which is then excluded from the fitting process. Once the best-fitting values of K^* are derived, we are able to evaluate N_{500} (out to $K = K^* + 2$) for each mock cluster and fit a power law of the form:

$$\log N_{500} = \alpha + \beta \log M_{500}. \quad (11)$$

As described in Section 4.2, the choice for using such a simple relation for fitting the data points in our plot, is justified by the fact we analyse only satellite galaxies within haloes of mass ($M_{200} > 10^{14} M_{\odot}$) significantly higher than the cut-off halo mass ($\gtrsim 10^{12} M_{\odot}$) introduced in the models (e.g., Kravtsov et al. 2004; Zheng, Coil & Zehavi 2007).

In this way we are able to investigate the slope of the $N_{500} - M_{500}$ relation and compare the obtained value from the simulations, with those obtained in the literature. This process is carried out for each of the aforementioned simulation snapshots, allowing us to study the evolution of the slope β of the $N_{500} - M_{500}$ relation with cosmic time. The best-fit values of β are reported in Table 3.

In order to investigate the evolution of the mean number of satellite galaxies $\langle N_{500} \rangle$ per halo mass with cosmic time, we restrict ourselves to the average values ($\langle N_{500} \rangle$; $\langle M_{500} \rangle$) for the 100 most massive clusters in each snapshot and carry out the same process utilized for the observed sample, now based on the stacked LF of the mock clusters. The values of $\langle N_{500} \rangle$ obtained are reported in Table 3 and plotted against M_{500} in Fig. 5.

5.3 Concentration Parameter

For each set of mock clusters, the value of c_g is also calculated using the same maximum-likelihood fitting procedure used for the observed clusters. The model used for the fitting procedure is similar to that described in Section 4.2.2, but with $\Sigma_{back} = 0$ (see Eq. 9), since the mock clusters do not suffer from contamination by galaxies not belonging to them due to the unambiguous way they are assigned to the mock haloes. The fitting procedure is applied to all the clusters individually (see Fig. 7) and also applied to the stacked projected number density profiles, which are first normalized to the virial area within R_{200} (see Table 3). Although at a given halo mass, the concentration parameters are commonly assumed to be lognormally distributed (e.g., Jing 2000; Neto et al. 2007; Comerford & Natarajan 2007), we prefer in this work to use the average values of c_g from the stacked profiles to compare with observations because the stacking procedure has the advantage of erasing individual deviations, usually related to the presence of substructure (Gao et al. 2008). These deviations may contribute to the already considerable intrinsic scatter (Neto et al. 2007 treated this issue in details) in the parameters fitted to individual profiles, possibly masking underlying trends in the data. It is worth pointing out that for the stacked profiles only the radial range $0.05 < R/R_{200} \lesssim 0.65$ is used in the fitting process in order to avoid the innermost radial region where the NFW model fails to correctly reproduce the density profile, as shown in several studies in the literature (e.g., Navarro et al. 2004; Prada et al. 2006 and Gao et al. 2008). The best fit values of the average c_g are reported in Table 3.

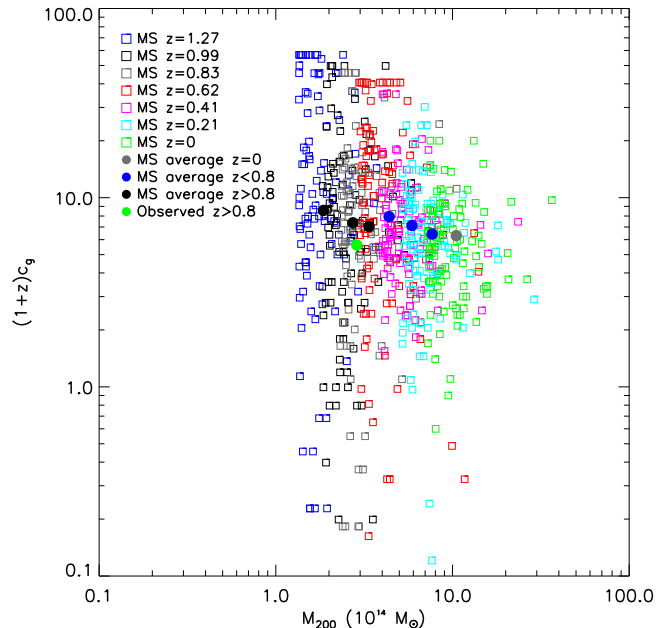


Figure 7. $(1+z)c_g$ against M_{200} . Measures of c_g are derived individually for the 100 most massive mock clusters in each of the considered snapshots. They are plotted as: blue squares ($z = 1.27$), black squares ($z = 0.99$), grey squares ($z = 0.83$), red squares ($z = 0.62$), magenta squares ($z = 0.41$), cyan squares ($z = 0.21$), green squares ($z = 0$). Average values are plotted as well: black full dots (mock clusters with $z > 0.8$), blue full dots (mock clusters with $z < 0.8$), grey full dot (mock clusters with $z = 0$), green full dot (observed clusters).

6 RESULTS

6.1 Evolution of K^*

The K^* values for our 15 clusters in the 3 redshift bins 0.85, 0.97, 1.23 are shown in Table 2 and compared to other results in Figure 4. Our values of K^* are consistent with other observations at similar wavelengths of other high-redshift clusters (e.g., De Propris et al. 1999; Ellis & Jones 2004; Strazzullo et al. 2006; Andreon 2006; Muzzin et al. 2007a). From a direct comparison with the K^* values predicted from our analysis of the mock clusters in the SAMs of Bower et al. (2006), we find good agreement: indicating, for the first time, that the SAMs do a reasonable job of predicting K^* evolution in rich clusters at redshifts $z \geq 1$. However, our data cannot distinguish between the mass-assembly SAMs and pure passively evolving SSP models with formation redshift $z_f \simeq 5$, implying that red, old massive galaxies are already ubiquitous in rich clusters at $z \simeq 1.5$.

6.2 HOD

6.2.1 Observations

The observed $\langle N_{500} \rangle$ values measured from our clusters ($0.8 \lesssim z \lesssim 1.5$) are shown in Fig. 5, where the local data from 93 clusters from Lin, Mohr & Stanford (2004) are also plotted along with their best-fit $N_{500} - M_{500}$ line. At all

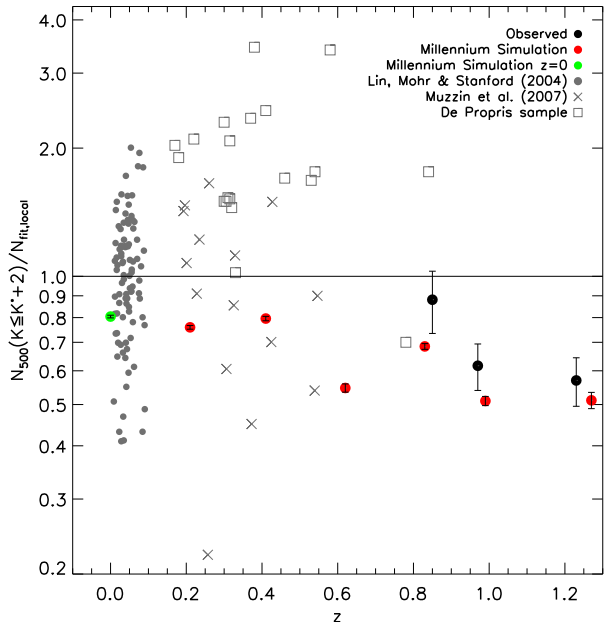


Figure 8. Ratio of measured N_{500} over the prediction of the low- z best-fitting relation of Lin, Mohr & Stanford (2004), against z : observed clusters (black full dots), mock clusters with $z > 0$ (red full dots), mock clusters with $z = 0$ (green full dot), Lin, Mohr & Stanford (2004) data points (grey full dots), De Propriis et al. (1999) sample as reanalysed by Lin, Mohr & Stanford (2004) (empty squares), Muzzin et al. (2007b) (crosses, note these values are extrapolated out to $K^* + 3$). Note our simulations based measures are average values measured over the 100 most massive clusters in each snapshot.

redshifts our points lie below the local fit. In Figure 8 we show the variation of $\langle N_{500} \rangle$ with redshift. Here the values of N_{500} have been normalised to the low- z best-fit relation shown in Figure 5 using the relation showed in Table 1 (second row) in Lin, Mohr & Stanford 2004 (see also Fig. 9 in their paper). The values measured for our clusters have $0.35 \lesssim N_{500}/N_{\text{fit,local}} \lesssim 0.8$. This result is in stark contrast to the results of the re-analysis by Lin and collaborators of the De Propriis et al. (1999) intermediate- z cluster sample, also shown in Figure 8, which indicate normalised N_{500} values typically between 1 – 4 for clusters in the range $0.2 < z < 0.8$. However, our results are consistent with those of Muzzin et al. (2007b), who carried out a similar study to ours on 15 CNOC1 clusters at $0.19 < z < 0.55$, and of Andreon et al. (2008), who found evidence of a possible break of the cluster scaling relations at $z \sim 1$.

To quantify the dependence of N_{500} on z and cluster mass in our data, we fit the N_{500} data to the relation used by Lin et al. (2006), and given by

$$N(M, z) = N_0(1+z)^\gamma (M/M_0)^s, \quad (12)$$

where N_0 and M_0 (set at $10^{14.3} M_\odot$ as in Lin et al. 2006) are the normalization factors of the relation. In the fit we use our binned results for the 15 high redshift clusters and the 93 low redshift data points of Lin, Mohr & Stanford 2004. The best-fitting values are $N_0 = 53 \pm 1$, $\gamma = -0.61^{+0.18}_{-0.20}$ and $s = 0.86 \pm 0.05$. Figure 9 shows the contours corresponding

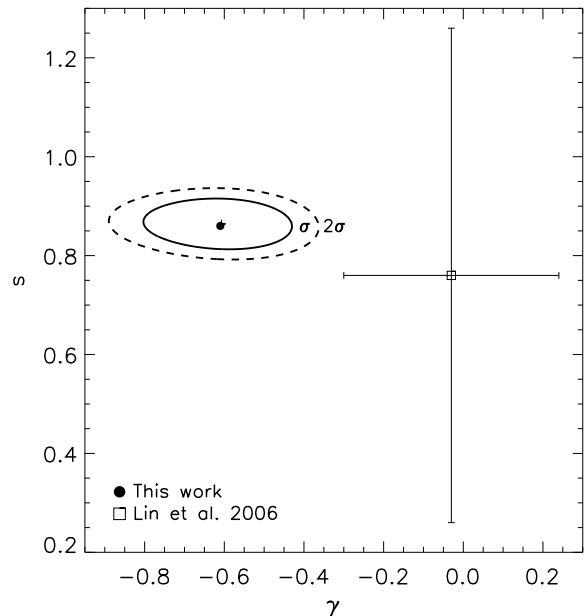


Figure 9. Joint 68 and 95 per cent confidence regions for γ and s (see eqn. 12). Black full point shows the best-fitting value for γ and s ($-0.61, 0.86$), while the cross stands for the center of the contours obtained during the marginalisation. Empty square represents the best-fitting values of γ and s (plotted together with their 1σ errors) by Lin et al. (2006) when including also the low- z cluster sample used here, in addition to their intermediate- z cluster sample.

to the 68 and 95 per cent confidence regions for γ and s . The quoted errors on γ and s are calculated by projecting the 68 per cent contour onto γ and s axes respectively.

Comparable measurements at our redshifts are those of Lin et al. 2006 who analysed 27 clusters with $0 < z < 0.9$. Our s value agrees reasonably well with their estimate ($s \simeq 0.8 \pm 0.5$) although evidence for an evolutionary trend in their data is significantly weaker ($\gamma = -0.03 \pm 0.27$). In fact, our value of γ indicates a significant trend with z at $\sim 3\sigma$ level; although with only 3 points at $z \geq 0.85$ more data and better redshift sampling are required to establish accurate trends. We are in fact also consistent with Lin et al. (2006) at $\sim 2\sigma$ level. Unfortunately we cannot test our results by using Lin et al. (2006) data points to repeat our fit, since their values are calculated within R_{2000} .

Turning to the study of the concentration parameter, the value of $c_g = 2.8^{+1}_{-0.8}$ found for the observed sample at $z \sim 1$, is consistent within 1σ with the one of Lin, Mohr & Stanford (2004) at $z \sim 0.06$ ($c_g = 2.90^{+0.21}_{-0.22}$). However, the latter value is quite different from the ones measured at similar redshifts (e.g., Rines & Diaferio 2006). In Figure 10 the current measure of c_g is plotted, together with the values found in the literature, as a function of $\log(z+1)$.

A comparison with the predictions of Gao et al. (2008) for dark matter haloes (see Section 6.2.2) at the same redshift as the median of the clusters studied here is also carried

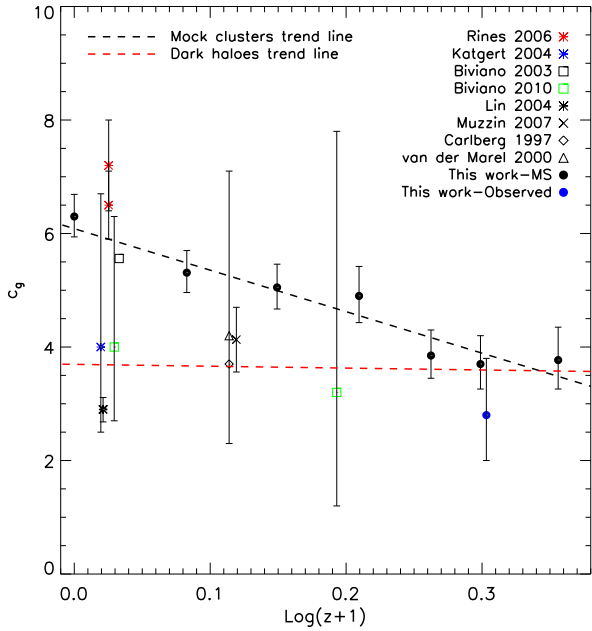


Figure 10. Average galaxy concentration parameter against $\log(z+1)$: this work (black full dots for mock clusters and blue full dot for our observed sample), Rines & Diaferio (2006) (red asterisks), Katgert, Biviano & Mazure (2004) (blue asterisk, slightly shifted towards lower z to improve data point visibility), Biviano & Girardi (2003) (black empty square), Biviano & Poggianti (2010) (green empty squares), Lin, Mohr & Stanford (2004) (black asterisk), Muzzin et al. (2007a) (black crosses, slightly shifted towards higher z for clarity), Carlberg et al. (1997) (black empty rhombus), van der Marel et al. (2000) (black empty triangle). Note for mock clusters, the 100 most massive clusters in each snapshot are used for this measure. Trend lines for the simulation-based average values of c_g measured in this work (black dashed line) and for the predictions of Gao et al. (2008) derived for dark matter haloes with the same halo masses as our mock clusters (red dashed line) are also plotted.

out, showing that our value of $c_g = 2.8_{-0.8}^{+1}$ is consistent with this prediction ($c_{\text{dm}} = 3.55$) (see Fig. 10).

6.2.2 Observations & Simulations: Most Massive Clusters

Turning to the results obtained for the simulations, the values of N_{500} measured from mock clusters ($0 < z < 1.3$) confirm the picture shown by the observed sample. In fact, as for the observed clusters, all the simulation-based values of N_{500} are lower than those predicted by the low- z best-fitting relation of Lin, Mohr & Stanford (2004), unlike those measured by Lin et al. for the sample of De Propris et al. (1999) (Figs. 5 & 8, Table 3).

When the evolution of β with z , as determined from mock cluster samples (Fig. 11), is studied, the values obtained seem to reveal no significant evolution with z (as also indicated by a Spearman's rank correlation test, which gives a correlation coefficient of $r = -0.2$ with a significance of its deviation from zero $p = 0.6$).

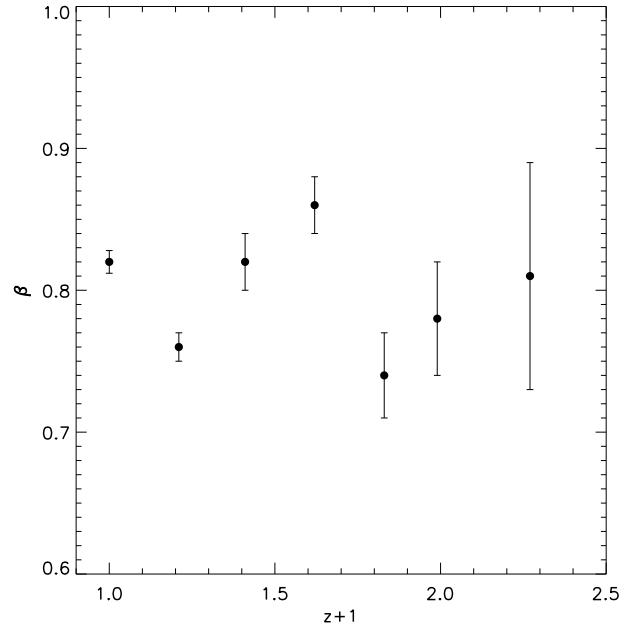


Figure 11. Halo HOD power-law index, as measured from mock clusters in each snapshot, against $(z+1)$. Note all the clusters with $M_{200} > 10^{14} M_{\odot}$ in each snapshot are used to carry out this measure.

The value measured at $z = 0$ ($\beta = 0.820 \pm 0.008$) is consistent with the ones of Lin, Mohr & Stanford (2004), Muzzin et al. (2007b) and Popesso et al. (2007). Despite this, as noted in the introduction, many studies, e.g. Magliocchetti & Porciani (2003); Zehavi (2004); Rozo et al. (2007) and Poggianti et al. (2010), measure discordant β values ranging from $\beta = 0.55 \pm 0.043$ (Marinoni & Hudson 2002) to $\beta = 1.1 \pm 0.09$ (Kochanek et al. 2003). Particularly high are the values found by Abbas et al. (2010), who, depending on the magnitude depth used and the redshift ($0.1 < z < 1.3$), found $0.99 \pm 0.10 < \beta < 1.66 \pm 0.18$. However, the majority of the studies in the literature agree with β being inconsistent with unity (this might not be the case for some other simulation-based studies, but a meaningful comparison with these studies is particularly hard).

In order to compare the results obtained for cluster galaxies with dark matter, the predictions of the $c_{\text{dm}}(z, M)$ relation obtained by Gao et al. (2008) within the MS can be used as a reference. Gao and collaborators presented in their study best-fitting $c_{\text{dm}}(M_{200})$ relations at $z = 0, 0.5, 1, 2$ and 3. To carry out this comparison, the values of c_{dm} predicted by their model are calculated using the values of \bar{M}_{200} at $z = 0, 0.62$ and 0.99 for our MS mock clusters (Table 3, Fig. 10) and at $z \sim 1$ for our observed cluster sample ($c_{\text{dm}} = 3.55$). This makes it possible to calculate $\Delta \log c = \log(c_g/c_{\text{dm}})$ (Zheng & Weinberg 2007) at each of the chosen z (Table 3) and to compare galaxy spatial distribution with the one of dark matter (a positive value of $\Delta \log c$ would mean galaxies are more clustered than dark matter and vice versa for negative values). This test shows

that $\Delta \log c$ decreases with redshift, reaching negative ($\Delta \log c = -0.1$, observed sample) or null ($\Delta \log c = 0$, mock clusters) values at $z \sim 1$. At this z , the value of $\Delta \log c$ is < 5 per cent of its value at $z = 0$.

6.2.3 Simulations: The Effect of Mass Selection

The results for N_{500} and c_g shown in the previous sections are acquired using mock samples which have an increasing mean cluster mass with cosmic time (see Table 3). As a result it is possible that this mass evolution affects the evolution of the HOD with cosmic time. In order to investigate this we repeat our analyses on two further mock samples of 100 clusters per snapshot: (i) selected within a constant mass range over cosmic time, set by the high- z sample; (ii) selected to have the same average mass at $z = 1$ and $z = 0$. We discuss the results from these samples below.

(i) We repeat our analysis on 100 mock clusters per snapshot randomly selected within the mass range of our observed cluster sample ($0.4 < M_{500} < 6.2 \times 10^{14} M_\odot$). The values of the average masses of these mock cluster samples are $M_{500} = 1.58, 1.45, 1.34, 1.21, 1.12, 1.06$ and $1.04 \times 10^{14} M_\odot$ at $z = 0, 0.21, 0.41, 0.62, 0.83, 0.99$ and 1.27 , respectively. When using these new mock clusters, we find very similar results to those described in Section 6.2.2 for the 100 most massive mock clusters at each snapshot. In particular we find $N_{500}/N_{\text{fit,local}}$ is always < 1 and for the 7 previously mentioned snapshots we find: $N_{500}/N_{\text{fit,local}} = 0.39 \pm 0.02, 0.42 \pm 0.02, 0.45 \pm 0.02, 0.49 \pm 0.03, 0.35 \pm 0.03, 0.37 \pm 0.03$ and 0.53 ± 0.03 respectively.

We also recalculate the average concentration parameter using the $z = 0$ and $z = 1.27$ snapshots and again reproduce similar results within the errors: $c_g = 4.7^{+0.97}_{-0.81}$ at $z = 1.27$ and $c_g = 8.7^{+1.6}_{-1.3}$ at $z = 0$.

(ii) As an additional test, we select mock clusters in the two redshift snapshots corresponding to $z = 0$ and $z = 1.0$. At both these redshifts we generate a sample of 100 mock clusters, selected at random from a Gaussian centered at $M_{500} = 2.1 \times 10^{14} M_\odot$, with a width given by the dispersion of our observed high-redshift clusters. Recomputing values in the same way as described in Section 6.2.2, we find $\langle N_{500} \rangle_{z=1} = 28 \pm 1$ at $z = 1$ and $\langle N_{500} \rangle_{z=0} = 36 \pm 1$ at $z = 0$. Normalising to the low- z relation of Lin, Mohr & Stanford (2004) as before (see Fig. 8), we find again values less than 1: $N_{500}/N_{\text{fit,local}} = 0.62 \pm 0.02$ and $N_{500}/N_{\text{fit,local}} = 0.5 \pm 0.02$ at $z = 0$ and $z = 1$ respectively.

For the concentration parameter we get $c_g = 7.5^{+0.96}_{-0.85}$ and $c_g = 3.7^{+0.5}_{-0.44}$ at $z = 0$ and $z = 1$, respectively. These results lie no more than $1 - 2\sigma$ from the values at the corresponding redshift snapshots shown in Fig. 10, while the larger errors reflect the increase in Poisson noise due to the smaller number of galaxies in less rich clusters, which are more numerous in samples characterised by lower average masses.

The results obtained here for N_{500} and c_g are both consistent with the simulation-based measurements in Fig. 8 and Fig. 10 respectively, which were based on mock samples

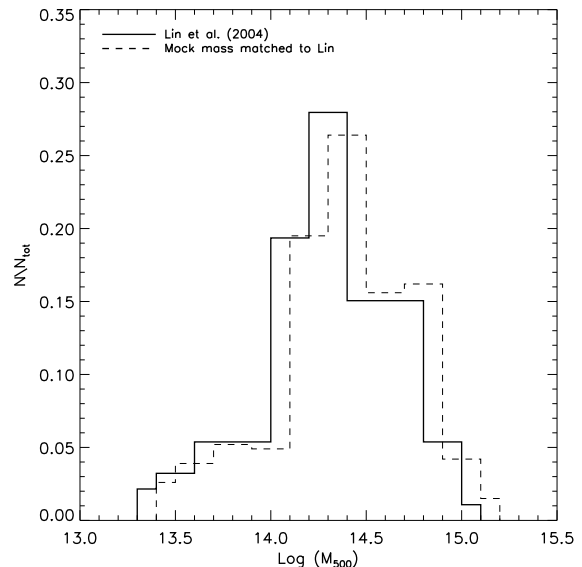


Figure 12. Mass distributions of Lin, Mohr & Stanford (2004) cluster sample (full line) and its mass matched counterpart in the mocks (dashed line, offset of 0.1 dex toward higher masses for clarity). See text for a description of the latter sample.

whose average mass changes with epoch. They demonstrate the robustness of our claim that high- z mock clusters agree with observations in hosting smaller numbers of galaxies compared to previous results and the claim of a significant evolutionary trend for c_g . This conclusion is supported by other evidence in the literature which shows that the dependence of the concentration parameter on mass is weak for haloes more massive than $10^{14} M_\odot$, e.g. Gao et al. (2008).

Finally, we note that the HOD power-law index β evolutionary analysis shown in Fig. 11 uses all clusters above $M_{200} = 10^{14} M_\odot$, in order to maximise the mass range and increase the signal given the large intrinsic scatter of the $N - M$ relation, with the consequence that the average mass in any of the 7 redshift snapshots varies by less than 30 per cent from the overall average across all snapshots.

6.2.4 Simulations: A Direct Comparison with Lin et al. at $z = 0$

The mock sample at $z = 0$ formed by the most massive haloes has a mass range ($5.2 < M_{500} < 26.0 \times 10^{14} M_\odot$) which only partially overlaps with that of Lin, Mohr & Stanford (2004) ($0.2 < M_{500} < 12.6 \times 10^{14} M_\odot$), resulting in a lack of haloes in the mocks less massive than $\sim 5 \times 10^{14} M_\odot$. To investigate whether this disparity in the mass range is related to the large difference we find between our $z = 0$ mock value of c_g and that of Lin, Mohr & Stanford (2004), we generate 1000 clusters selected randomly from Lin's accumulated mass distribution and associate each of them with the $z = 0$ mock cluster closest in mass. This produces a mock cluster sample closely matched to Lin, Mohr & Stanford (2004); see Figure 12. When using the new mock sample described we obtain

$c_g = 8.0_{-0.31}^{+0.32}$, which is again consistent with the previous results for the low- z mocks and significantly different from the value ($c_g = 2.9_{-0.22}^{+0.21}$) of Lin, Mohr & Stanford (2004).

7 DISCUSSION

From our study of the evolution of K^* , shown in Fig. 4, it is evident that the SAMs reproduce the K^* values of our high redshift clusters reasonably well. The data points of Cirasuolo et al. (2007) and the parameterized fit of the evolution of K^* from Cirasuolo et al. (2010) for the field LF are also plotted in this Figure. It can be seen there is a small difference of, on average, $\Delta K^* \sim 0.5$ at $z > 0.8$ between the cluster environment (brighter K^*) and the field. Furthermore, Balogh et al. (2001) found in their study of the J -band LF a difference of similar magnitude between cluster and field of $\Delta J^* \sim 0.5$. The results of Cirasuolo et al., are from a sample of 50,000 galaxies with photometric redshifts $0.25 \leq z \leq 3.25$ from the UKIDSS UDS in which they compare the K -band LF with the predictions of SAMs (including Bower et al. 2006) finding broad consistency - even though some models still tend to under predict the number of field galaxies at high z . However, we point out that the Bower et al. (2006) SAM does a better job of predicting the number of high- z field galaxies than other SAMs. Although our study is restricted to the analysis of K^* , it is clear that our results indicate that the current SAMs can predict the luminosities of L^* galaxies both in the field and rich clusters, where substantially more merging has taken place, reasonably well. On the other hand some authors (e.g., Cimatti, Daddi & Renzini 2006; Pozzetti et al. 2010) have pointed out that the massive end of the galaxy mass function does not appear to evolve significantly since $z \sim 1$ and questioned whether downsizing is compatible with the predictions of SAMs. As mentioned in the introduction, the situation is potentially even worse for BCGs at the centre of rich clusters. In fact, Collins et al (2009) and Stott et al (2010) showed that the observed stellar mass of BCGs in high-mass X-ray clusters does not evolve significantly since $z \simeq 1.5$, in contrast with the SAMs which predict that BCGs at this redshift should only have 20–30 per cent of the stellar mass of their local counterparts.

These results, taken together with the small difference between observed field and cluster K^* values, now confirmed here, (see also Cole et al. 2001; De Propriis & Christlein 2009) and together with other evidence found in the literature that the luminous ($L > L^*$) part of the LF weakly depends on the environment (e.g., Cimatti, Daddi & Renzini 2006; De Filippis et al. 2011), indicates that the hierarchical galaxy formation scenario works well for galaxies up to a mass $M \sim 10^{11} M_\odot$ (about the mass of an L^* galaxy).

Our halo HOD power-law indexes ($\beta \simeq 0.8$) for mock clusters are in agreement with several studies in the literature, e.g. Lin, Mohr & Stanford (2004), Muzzin et al. (2007b) and Popesso et al. (2007). However, the picture is complicated, since several other studies such as Kochanek et al. (2003) and Poggianti et al. (2010), found values of β greater than or consistent with 1. As emphasized by Popesso and collaborators and Lin et al., a value $\beta < 1$ is expected from the theoretical point of view. This is

because, despite the fact that the hierarchical structure formation models (e.g. De Lucia et al. 2004; Gao et al. 2004) predict a universal mass distribution of sub-haloes (independent of the parent halo’s mass and with the consequence that the number of sub-haloes is proportional to halo mass), the introduction of baryons produces a decreasing number of galaxies per unit mass (e.g., Berlind et al. 2003) and an increasing M/L ratio (e.g., Kauffmann et al. 1999) for higher halo masses. Several processes may be responsible for this behavior, such as an increased merger rate (White, Hernquist & Springel 2001) or an increasing galaxy destruction rate (Lin, Mohr & Stanford 2004) or decreasing star formation and gas cooling efficiencies (e.g., Berlind et al. 2003). However, as pointed out by Popesso et al. (2007), each of these processes should leave their mark in the properties of galaxy clusters. Lin, Mohr & Stanford (2004) split their sample into a high and low-mass sub-samples and found both an excess and a lack of galaxies in the faint and the bright parts of the LF respectively for the low-mass cluster sub-sample, although they concluded that none of the studied processes (tidal stripping, ram pressure stripping, galaxy harassment, variations in star formation efficiency, stellar aging, differences in galaxy radial distribution, dynamical friction and galaxy mergers) can by itself satisfactorily explain these differences. On the other hand, Popesso et al. (2007) found a universal LF with no dependence on the cluster mass and wave-band. For this reason, they proposed the only way to have $\beta < 1$ leaving the properties of galaxy clusters unchanged is if the sub-haloes mass distribution is not universal. It is beyond the scope of the present study to address which process may cause $\beta < 1$ or whether the sub-haloes mass distribution is universal and we simply point out that our analysis on mock clusters shows no significant evolution of β with z ($\beta \sim 0.8$ out to $z \sim 1.3$) and that whatever this process might be, it is already in place by $z \sim 1$.

Our observational-based results indicate that low- z clusters are richer than their high- z counterparts when comparing clusters of the same mass. Using the best fit relation to Eq. 12 and the masses in Table 3, N_{500} increase by a factor of ~ 1.6 from $z \sim 1$ to $z \sim 0.6$ and by a factor of ~ 2.6 from $z \sim 0.6$ to $z = 0$. This growth rate of the number of galaxies is very similar to the one found by Abbas et al. (2010) over a similar redshift interval.

Using mock clusters, Poggianti et al. (2010) also found little evolution in the β value for their samples, although pointed out that values can depend on whether masses of mock clusters are derived from their intrinsic halo mass ($\beta = 1.00 \pm 0.04$) or using their velocity dispersion mass proxy ($\beta = 0.77 \pm 0.03$). It is not possible to match our X-ray measurements to the simulations in the same way at the present time but clearly further work is necessary to compare different mass estimators. However, we point out that we obtain an average value of $\beta < 1$ for our mock clusters despite using the halo mass values provided by the simulation.

Focusing the attention on the galaxy concentration parameter (Table 3 and Figs. 6 & 10), the present analysis leads to a picture which is difficult to fully un-

derstand, partly due to the diversity of the c_g found in the literature (Carlberg et al. 1997; van der Marel et al. 2000; Biviano & Girardi 2003; Katgert, Biviano & Mazure 2004; Lin, Mohr & Stanford 2004; Rines & Diaferio 2006; Muzzin et al. 2007a; Biviano & Poggianti 2010), whose large scatter is probably due to the heterogeneity of the analysis methods, which are often based on different radial distances and magnitude limits. Another possible cause of this large scatter could be the cluster-to-cluster variation, which can influence the headline value of c_g when simply averaging over individual measurements (using individual surface density profiles), as opposed to the preferred method of fitting the stacked density profile. However, we note that the most accurate c_g estimate on intermediate z scale ($c_g = 4.13 \pm 0.57$), carried out by Muzzin et al. (2007a) and based on redshift measurements, agrees well with our observations at $z = 1$. The values of c_g measured for our mock clusters are seen to increase with decreasing redshift, giving rise to a significant correlation with a Spearman rank correlation coefficient of -0.96 . In particular, those obtained for high- z mock clusters ($c_g = 3.85_{-0.4}^{+0.45}$, $3.70_{-0.44}^{+0.5}$ and $3.77_{-0.51}^{+0.58}$ at $z = 0.83$, 0.99 and 1.27 , respectively) are found consistent within 1σ with the value of $c_g = 2.8_{-0.8}^{+1}$ found for our observed sample at $z \sim 1$. The large errors characterising the observed values found in the literature, do not allow us to address this issue in a more quantitative way. Having said that, when the value obtained for mock clusters at $z = 0$ ($c_g = 6.30_{-0.36}^{+0.39}$) is compared with the observed one of Lin, Mohr & Stanford (2004) ($c_g = 2.90_{-0.22}^{+0.21}$) at $z \sim 0.06$, the discrepancy appears large and significant, although the models agree with other low- z observation-based estimates of c_g . If real, this would be an indication that SAMs have problems in predicting the evolution of cluster galaxies observed from $z \sim 1$ to $z = 0$.

A potentially very important difficulty which arises in the simulations is the problem of the *orphan* galaxies (Shaun Cole, private communication). These are galaxies which have lost their dark matter haloes and whose tracks in the simulations are traced by following the particle that was the one most bound in its halo prior to disruption. In the Bower et al. (2006) SAM, the merging of satellites onto the central galaxy is treated using a dynamical friction calculation that, instead of using the true orbit of the galaxy, uses random orbital parameters that are only statistically consistent with N-body simulations. This could lead to biasing the concentration parameter towards higher values. In fact, in reality, the satellites most likely to merge are the ones on orbits closest to the centre, whereas random selection in the SAM of Bower et al. removes satellites randomly at all radii. Hence, the remaining satellites may be too concentrated. While there is no reason to expect that the current treatment of satellite galaxy mergers should give rise to the entire trend seen in Fig. 10, the possibility cannot be ruled out. This issue will only be decided by carrying out a more accurate treatment of the merging and orbits of satellite galaxies, which has already been developed, but not yet applied to the MS. However, it is worth pointing out that the problems of calculating the radial distribution of satellite galaxies in the Bower et al. (2006) model are not expected to lead to significant errors

in the numbers of satellite galaxies contributing to the HOD.

The growth of mock c_g with decreasing z seen in the present analysis is not unexpected. What is surprising, instead, is the rate of this growth. Investigating dark matter haloes within simulations, studies like Neto et al. (2007); Gao et al. (2008); Duffy et al. (2008) and Muñoz-Cuartas et al. (2011) addressed the $c_{\text{dm}}(z, M)$ relation in details finding c_{dm} being anti-correlated with mass and z . In particular, the anti-correlation between c_{dm} and M weakens at higher z and evidence of dark matter haloes having a constant $c_{\text{dm}} \sim 3.5 - 4$ at $z > 1$ have been found by Gao et al. (2008).

Comparing the mock-cluster values of c_g measured here with the ones of the dark matter haloes predicted by theoretical studies (Gao et al. 2008) at different z (see Section 6), the results seem to show that galaxies have a similar concentration to dark matter at $z \sim 1$ but subsequently they become more concentrated with decreasing redshift. This may be due to the effect of non-gravitational or gravitational processes, such as: gas cooling, AGN feedback, dynamical friction, merging and tidal stripping, which have significantly modified the galaxy distribution within the dark matter halo over the last ~ 9 Gyr. This growth is dominated by the continuously refined physics of the SAMs (e.g., Duffy et al. 2010), and given this sensitivity, a glance at the data in Fig. 10 suggests the need for a thorough and homogeneous study of c_g in observed galaxy clusters and groups over a wide range in redshift.

8 CONCLUSIONS

We study the evolution of cluster galaxies with z using K -band photometry of a cluster sample made of 15 of the highest- z ($0.8 < z < 1.5$) X-ray clusters observed so far. In particular, we investigate the K^* Hubble diagram out to $z \sim 1.3$ in comparison with SSP (no evolution in absolute K -band magnitude and passive evolution) and SAM evolutionary models. This allows us to explore the process of galaxy formation. We also study the HOD of this sample, by investigating $\langle N \rangle$, as a function of M and z , and c_g with z in comparison with c_{dm} . All our analysis is carried out in strict comparison with simulations, through the use of mock cluster samples taken from MS at $0 < z < 1.3$ and populated with galaxies by means of the SAM by Bower et al. (2006). In addition to being an important test for SAMs, this allows us to investigate in details the evolution of β , $\langle N \rangle$ and c_g with z and to study how the relationship between galaxies and dark matter spatial distributions within haloes changes with cosmic time. This kind of study is fundamental for understanding the role non-gravitational processes, as part of the physics of galaxy formation, take in influencing the way galaxies populate dark matter haloes. Our main conclusions are:

- (i) The values of K^* obtained show the existence of old, evolved and massive galaxies at $z > 1.5$. Despite the evolution of K^* is well reproduced by SSP passive evolutionary models ($z_f > 3$), we can not disentangle between these models and the predictions of Bower et al. (2006) SAM,

which is seen, for the first time, to reproduce well the evolution of K^* also in the cluster environment.

(ii) When comparing the values of K^* obtained for observed clusters with the ones of the field, there are no major differences. This fact, coupled with the marginal evolution of the massive end of the galaxy mass function seen observationally (e.g., Cimatti, Daddi & Renzini 2006; Pozzetti et al. 2010), leads to questioning whether the role of the environment is negligible for the formation of galaxies more massive than $\sim 10^{11} M_{\odot}$ (about the mass of a L^* galaxy).

(iii) By investigating N_{500} in real and mock clusters, this study shows that high- z clusters are poorer than those at low z . Unlike Lin et al. (2006), we find significant trends of N_{500} with both z and cluster mass: $N(M, z) = (53 \pm 1)(1 + z)^{-0.61^{+0.18}_{-0.20}}(M/10^{14.3})^{0.86 \pm 0.05}$.

(iv) Using mock clusters, the slope β of the $N_{500} - M_{500}$ relation is found to be significantly lower than one at all z (out to $z \sim 1.3$), showing no significant signs of evolution. This means more massive clusters are characterized by a lower galaxy number per unit mass compared to lower mass systems already at high z . Because of this, the local value of $\beta < 1$ can not be explained as being due to local clusters found to be richer than those at high- z .

(v) Although our results here and those from the literature seem to indicate a decreasing trend of c_g with z , overall the data and SAM-based predictions are very uncertain and the current situation emphasizes the compelling need of a systematic and homogeneous study of the galaxy concentration parameter in clusters over low and intermediate redshifts.

(vi) When comparing our mock-cluster values of c_g (3.7-6.3) with those of c_{dm} (3.6-3.8), starting from similar concentrations at $z \sim 1$, galaxies seem to become more concentrated than dark matter as z approaches 0. This may be due to gravitational and/or non-gravitational processes significantly modifying the distribution of galaxies within dark matter haloes over the last ~ 9 Gyr. However, the problem of the *orphan galaxies* in the SAMs prevents us concluding that this is a real physical trend.

Acknowledgments

The authors thank the referee Cedric Lacey for a report which significantly improved the paper. We also thank Shaun Cole for the useful discussion about the SAM models and Adam Muzzin for kindly providing his data. DC expresses his gratitude to Ivan Baldry and Maurizio Paolillo for the valuable discussions and support. DC also thanks Gerard Lemson for the helpful suggestions with regards to the MS database. CAC and JPS acknowledge financial support from STFC. MH acknowledges financial support from the Leverhulme Trust. This work is based in part on data collected at the Subaru Telescope, which is operated by the National Astronomy Observatory of Japan and the XMM-Newton, an ESA science mission funded by contributions

from ESA member states and from NASA.

IRAF is distributed by the National Optical Astronomy Observatories, which are operated by the Association of Universities for Research in Astronomy, Inc., under cooperative agreement with the National Science Foundation.

REFERENCES

- Abbas U., et al., 2010, MNRAS, 406, 1306
 Andreon S., 2006, A&A, 448, 447
 Andreon S., De Propris R., Puddu E., Giordano L., Quintana H., 2008, MNRAS, 383, 102
 Balestra I., Tozzi P., Ettori S., Rosati P., Borgani S., Mainieri V., Norman C., Viola M., 2007, A&A, 462, 429
 Balogh M. L., Christlein D., Zabludoff A. I., Zaritsky D., 2001, ApJ, 557, 117
 Bartelmann M., 1996, A&A, 313, 697
 Benson A. J., Baugh C. M., Cole S., Frenk C. S., Lacey C. G., 2000, MNRAS, 316, 107
 Berlind A. A., Weinberg D. H., 2002, ApJ, 575, 587
 Berlind A. A. et al., 2003, ApJ, 593, 1
 Biviano A., Girardi M., 2003, ApJ, 585, 205
 Biviano A., Poggianti B., 2010, in American Institute of Physics Conference Series, Vol. 1241, American Institute of Physics Conference Series, J.-M. Alimi & A. Fuözfa, ed., pp. 192–199
 Bower R. G., Benson A. J., Malbon R., Helly J. C., Frenk C. S., Baugh C. M., Cole S., Lacey C. G., 2006, MNRAS, 370, 645
 Branchesi M., Gioia I. M., Fanti C., Fanti R., 2007, A&A, 472, 739
 Bremer M. N. et al., 2006, MNRAS, 371, 1427
 Bruzual G., Charlot S., 2003, MNRAS, 344, 1000
 Buote D. A., Gastaldello F., Humphrey P. J., Zappacosta L., Bullock J. S., Brighenti F., Mathews W. G., 2007, ApJ, 664, 123
 Capozzi D., Collins C. A., Stott J. P., 2010, MNRAS, 403, 1274
 Carlberg R. G. et al., 1997, ApJ Let., 485, L13+
 Christlein D., Zabludoff A. I., 2003, ApJ, 591, 764
 Cimatti A., Daddi E., Renzini A., 2006, A&A, 453, L29
 Cirasuolo M., McLure R. J., Dunlop J. S., Almaini O., Foucaud S., Simpson C., 2010, MNRAS, 401, 1166
 Cirasuolo M. et al., 2007, MNRAS, 380, 585
 Cole S., et al., 2001, MNRAS, 326, 255
 Colless M., et al., 2001, MNRAS, 328, 1039
 Collins C. A. et al., 2009, Nature, 458, 603
 Collister A. A., Lahav O., 2005, MNRAS, 361, 415
 Comerford J. M., Natarajan P., 2007, MNRAS, 379, 190
 Cowie L. L., Songaila A., Hu E. M., Cohen J. G., 1996, AJ, 112, 839
 De Filippis E., Paolillo M., Longo G., La Barbera F., de Carvalho R. R., Gal R., 2011, MNRAS, 414, 2771
 De Lucia G., Blaizot J., 2007, MNRAS, 375, 2
 De Lucia G., Kauffmann G., Springel V., White S. D. M., Lanzoni B., Stoehr F., Tormen G., Yoshida N., 2004, MNRAS, 348, 333
 De Lucia G., Springel V., White S. D. M., Croton D., Kauffmann G., 2006, MNRAS, 366, 499
 De Lucia G., et al., 2007, MNRAS, 374, 809

- De Propriis R., Christlein D., 2009, *Astronomische Nachrichten*, 330, 943
- De Propriis R., Eisenhardt P. R., Stanford S. A., Dickinson M., 1998, *ApJ Let.*, 503, L45+
- De Propriis R., Stanford S. A., Eisenhardt P. R., Dickinson M., Elston R., 1999, *AJ*, 118, 719
- Duffy A. R., Schaye J., Kay S. T., Dalla Vecchia C., 2008, *MNRAS*, 390, L64
- Duffy A. R., Schaye J., Kay S. T., Dalla Vecchia C., Battye R. A., Booth C. M., 2010, *MNRAS*, 405, 2161
- Ellis S. C., Jones L. R., 2004, *MNRAS*, 348, 165
- Gao L., Navarro J. F., Cole S., Frenk C. S., White S. D. M., Springel V., Jenkins A., Neto A. F., 2008, *MNRAS*, 387, 536
- Gao L., White S. D. M., Jenkins A., Stoehr F., Springel V., 2004, *MNRAS*, 355, 819
- Hashimoto Y., Barcons X., Böhringer H., Fabian A. C., Hasinger G., Mainieri V., Brunner H., 2004, *A&A*, 417, 819
- Hicks A. K. et al., 2008, *ApJ*, 680, 1022
- Hilton M., et al., 2010, *ApJ*, 718, 133
- Ho S., Lin Y.-T., Spergel D., Hirata C. M., 2009, *ApJ*, 697, 1358
- Hu W., Kravtsov A. V., 2003, *ApJ*, 584, 702
- Ichikawa T. et al., 2006, in *Society of Photo-Optical Instrumentation Engineers (SPIE) Conference Series*, Vol. 6269, *Society of Photo-Optical Instrumentation Engineers (SPIE) Conference Series*
- Jing Y. P., 2000, *ApJ*, 535, 30
- Katgert P., Biviano A., Mazure A., 2004, *ApJ*, 600, 657
- Kauffmann G., Colberg J. M., Diaferio A., White S. D. M., 1999, *MNRAS*, 303, 188
- Kochanek C. S., White M., Huchra J., Macri L., Jarrett T. H., Schneider S. E., Mader J., 2003, *ApJ*, 585, 161
- Kravtsov A. V., Berlind A. A., Wechsler R. H., Klypin A. A., Gottlöber S., Allgood B., Primack J. R., 2004, *ApJ*, 609, 35
- Lamer G., Hoefft M., Kohnert J., Schwöpe A., Storm J., 2008, *A&A*, 487, L33
- Lawrence A., et al., 2007, *MNRAS*, 379, 1599
- Leggett S. K., 1992, *ApJS*, 82, 351
- Lemson G., Virgo Consortium t., 2006, *ArXiv Astrophysics e-prints*: 0608019
- Lin Y., Mohr J. J., Gonzalez A. H., Stanford S. A., 2006, *ApJ Let.*, 650, L99
- Lin Y., Mohr J. J., Stanford S. A., 2004, *ApJ*, 610, 745
- Lubin L. M., Mulchaey J. S., Postman M., 2004, *ApJ Let.*, 601, L9
- Magliocchetti M., Porciani C., 2003, *MNRAS*, 346, 186
- Marinoni C., Hudson M. J., 2002, *ApJ*, 569, 101
- Martini P., 2001, *AJ*, 121, 598
- Maughan B. J., 2007, *ApJ*, 668, 772
- Maughan B. J., Jones L. R., Ebeling H., Scharf C., 2004, *MNRAS*, 351, 1193
- Maughan B. J., Jones L. R., Ebeling H., Scharf C., 2006, *MNRAS*, 365, 509
- McCracken H. J., et al., 2010, *ApJ*, 708, 202
- Muñoz-Cuartas J. C., Macciò A. V., Gottlöber S., Dutton A. A., 2011, *MNRAS*, 411, 584
- Muzzin A., Yee H. K. C., Hall P. B., Ellingson E., Lin H., 2007a, *ApJ*, 659, 1106
- Muzzin A., Yee H. K. C., Hall P. B., Lin H., 2007b, *ApJ*, 663, 150
- Nagai D., Kravtsov A. V., 2005, *ApJ*, 618, 557
- Navarro J. F., Frenk C. S., White S. D. M., 1997, *ApJ*, 490, 493
- Navarro J. F. et al., 2004, *MNRAS*, 349, 1039
- Neto A. F. et al., 2007, *MNRAS*, 381, 1450
- Peacock J. A., Smith R. E., 2000, *MNRAS*, 318, 1144
- Percival W. J., et al., 2001, *MNRAS*, 327, 1297
- Phleps S., Peacock J. A., Meisenheimer K., Wolf C., 2006, *A&A*, 457, 145
- Poggianti B. M., 1997, *A&AS*, 122, 399
- Poggianti B. M., De Lucia G., Varela J., Aragon-Salamanca A., Finn R., Desai V., von der Linden A., White S. D. M., 2010, *MNRAS*, 405, 995
- Popesso P., Biviano A., Böhringer H., Romaniello M., 2007, *A&A*, 464, 451
- Pozzetti L., et al., 2010, *A&A*, 523, A13+
- Prada F., Klypin A. A., Simonneau E., Betancort-Rijo J., Patri S., Gottlöber S., Sanchez-Conde M. A., 2006, *ApJ*, 645, 1001
- Rines K., Diaferio A., 2006, *AJ*, 132, 1275
- Rosati P., et al., 2009, *A&A*, 508, 583
- Roze E. et al., 2007, *ArXiv Astrophysics e-prints*
- Schechter P., 1976, *ApJ*, 203, 297
- Skrutskie M. F., et al., 2006, *AJ*, 131, 1163
- Spergel D. N. et al., 2003, *ApJS*, 148, 175
- Springel V. et al., 2005, *Nature*, 435, 629
- Stott J. P. et al., 2010, *ApJ*, 718, 23
- Stott J. P., Smail I., Edge A. C., Ebeling H., Smith G. P., Kneib J.-P., Pimblet K. A., 2007, *ApJ*, 661, 95
- Strazzullo V. et al., 2006, *A&A*, 450, 909
- Temporin S., et al., 2008, *A&A*, 482, 81
- Thomas D., Maraston C., Bender R., Mendes de Oliveira C., 2005, *ApJ*, 621, 673
- van der Marel R. P., Magorrian J., Carlberg R. G., Yee H. K. C., Ellingson E., 2000, *AJ*, 119, 2038
- Vikhlinin A. et al., 2009, *ApJ*, 692, 1060
- Whiley I. M. et al., 2008, *MNRAS*, 387, 1253
- White M., Hernquist L., Springel V., 2001, *ApJ Let.*, 550, L129
- Yang X., Mo H. J., van den Bosch F. C., 2008, *ApJ*, 676, 248
- Zehavi, I. e. a., 2004, *ApJ*, 608, 16
- Zheng Z., Coil A. L., Zehavi I., 2007, *ApJ*, 667, 760
- Zheng Z., Weinberg D. H., 2007, *ApJ*, 659, 1